International Journal of Heat and Mass Transfer 221 (2024) 125078

Contents lists available at ScienceDirect

International Journal of Heat and Mass Transfer

journal homepage: www.elsevier.com/locate/ijhmt

High heat flux dissipation of membrane-venting heat sink with thin film boiling

Ji Li [a,b,1], Zikang Zhang [a,1], Yifan Zhang [a], Runze Zhao [a], Haichuan Cui [a], Tianyou Zhai [b], Wei Liu [a], Zhichun Liu [a,*]

[a] School of Energy and Power Engineering, Huazhong University of Science and Technology, Wuhan 430074, China
[b] State Key Laboratory of Materials Processing and Die and Mould Technology, School of Materials Science and Engineering, Huazhong University of Science and Technology, Wuhan 430074, China

ARTICLE INFO

Keywords:
Thermal management
Flow boiling
Microchannel
Membrane distillation
Thin liquid film

ABSTRACT

Microchannel flow boiling exhibits outstanding heat transfer capabilities, rendering it a promising technology for cooling high heat flux devices. Nonetheless, rapid vapor generation in the channels increases pressure drop and leads to local dryness, restricting the performance of microchannel heat sinks. In this study, we designed a membrane-venting heat sink that has a hydrophobic porous membrane above a thin liquid film for venting vapor. The phase change of this heat sink comprises not only thin film flow boiling in the horizontal direction but also thin film boiling and thin film evaporation in the vertical direction, thereby mitigating the detrimental effects of flow boiling. Experiments indicate that utilizing a membrane with 1.0 μm pore size for venting can enable the effective heat flux of the heat sink to achieve 287.8 W/cm^2, with a transmembrane heat flux of 152.7 W/cm^2. Furthermore, the surging trend of pressure drop with heat flux was significantly slowed down, and the maximum effective heat flux increased by 553 % compared to the configuration without vent. This study demonstrates that adding and enhancing the vertical heat and mass transfer channels via hydrophobic porous membranes is a potent method for considerably improving flow boiling.

1. Introduction

With the advancement of technologies such as chips, lasers, nuclear energy, and radar, the power density and the heat dissipation demands of devices are rapidly escalating, reaching up to hundreds of watts per square centimeter [1,2], For instance, insulated gate bipolar transistor (IGBT) devices' heat dissipation requirements have reached 100–150 W/cm^2 with expectations to rise to 500 W/cm^2 in future generations [3]. Traditional technologies struggle to dissipate such high heat flux. Consequently, the development of more efficient cooling methods is crucial. Heat dissipation technologies based on liquid convection or vaporization, including microchannels [4,5], heat pipes [6,7], pool boiling [8,9], thin film boiling [10,11], jet impingement [12,13], and spray [14,15], exhibit high heat transfer coefficients or critical heat flux resulting from utilizing the high sensible or latent heat of the liquid. Thus, these technologies garn substantial research interest.

Microchannel heat sinks typically feature multiple parallel micro-scale channels and fins. During operation, microchannel heat sinks can achieve high-efficient heat exchange as working fluid flows through these channels. Microchannel heat sinks have the advantages of simple design, compact structure, and long heat transport distance, leading to a wide range of applications [16]. For single-phase cooling of micro-channels under a certain flow structure, the heat transfer capacity mainly depends on the fluid flow rate. However, increasing the flow rate results in a rapid surge in pressure drop, making it difficult to control power consumption. When the working fluid flows from the inlet to the outlet of a microchannel, the phase change from liquid to vapor can occur due to temperature increases and pressure decreases. Under this condition, the working regime transitions to flow boiling, significantly enhancing the heat transfer and substantially reducing the demand for flow rate, thus, power consumption can decrease [17]. Nonetheless, under a high heat flux, the vapor volume fraction in the channel can become quite high, which may lead to a rapid increase in pressure drop and potentially offset the power consumption advantage. Additionally, it can result in local dryness and limit the critical heat flux [18,19],

To improve the heat and mass transfer characteristics of micro-channel flow boiling, structure optimization and surface modification

* Corresponding author.
E-mail address: zcliu@hust.edu.cn (Z. Liu).
[1] These author equal contribution to this work.

https://doi.org/10.1016/j.ijheatmasstransfer.2023.125078
Received 3 November 2023; Accepted 11 December 2023
Available online 16 December 2023

Nomenclature

A	cross-section area of sink base cm^2
C_p	specific heat of water J/kg°C
d	depth mm
D	diameter mm
h	height mm
H_{lv}	latent heat of vaporization J/kg
J_{mem}	transmembrane mass flux kg/m^2•s
k_{Al}	thermal conductivity of aluminum alloy 6063 201 W/m °C
l	length mm
m	mass of liquid reservoir kg
MV-TFB	membrane-venting thin film boiling
P	pressure kPa
PET	polyethyleneterephthalate
PTFE	polytetrafluoroethylene
Q_{in}	input heat power to heater W
Q_{eff}	effective heat power to heat sink W
Q'_{eff}	effective heat power to fluid W
Q_{loss}	heat loss rate W
q_{eff}	effective heat flux to heat sink W/cm^2
q_{mem}	transmembrane heat flux W/cm^2
SPC	single-phase convection
t	time s
thk	thickness mm
T	temperature °C
TPC-SCB	two-phase convection with subcooled boiling
TPC-STB	two-phase convection with saturated boiling
$\dot{V}$	inlet rate mL/min
$w$width	widthmm

Greek symbols

ρdensity of liquid water	density of liquid water kg/m^3
χ	vapor quality

Subscripts

in	inlet
max	maximum value
out	outlet
$wall$	wall of liquid plate

are two primary approaches. Cui et al. [4] fabricated rectangular microchannels with an ultrahigh aspect ratio, where the depth-to-width ratio is 25 and the sink has a larger heat transfer area. The flow boiling experiment showed that, compared to the microchannels with a ratio of 1, the critical heat flux can be increased by 40.95 % and the thermal resistance can be reduced by 40.28 % under the same flow rate. Deng et al. [20] designed a type of pin fin-interconnected reentrant microchannel heat sink, where the reentrant chambers facilitated nucleation and the pin fins improved vapor flow. Kandlikar et al. [21] proposed open microchannels with a tapered manifold. Experiments showed that the tapered manifold can suppress the backflow phenomenon during flow boiling. Priy et al. [22] arranged a vapor venting manifold at the exit of microchannels based on a hydrophobic porous membrane, thereby the evacuation of the bubbles was promoted and the backflow was also suppressed. Alam et al. [23] conducted flow boiling experiments on silicon bases with HFE-7100. They found that the microchannels with nanowire structures exhibited an up 400 % improvement in heat transfer coefficient compared to plain wall microchannels due to the superior wettability of nanowire structure, which can promote explosive boiling, thin liquid film evaporation, and annular flow. Jiang et al. [24] experimentally compared the improving effects of surface enhancements such as laser etching, nano-coating, and laser-drilling on microchannel flow boiling. The microchannels with laser-drilled cavities and nano-coating structures presented the best heat transfer performance, with a 98.6 % increase in heat transfer coefficient compared to bare wall microchannels. Yin et al. [25] conducted experiments comparing porous open microchannels and solid copper open microchannels for flow boiling. The heat transfer coefficient of porous open microchannels increased by nearly 100 % due to the nucleation sites and capillary wetting effect provided by sintering walls. Flow boiling experiments by Fu et al. [26] also demonstrated that the foam fin microchannels can have an 80 % higher heat transfer coefficient compared to solid fin microchannels with the same geometric dimensions, though along with a 20 % increase in pressure drop.

To improve the characteristics of microchannel flow boiling, inspiration can be obtained from other phase change technologies. Membrane distillation is a separation technology that can separate volatiles and non-volatile components of liquid based on the gas-permeation and liquid-repellent properties of the hydrophobic porous membrane [27]. David et al. [28] reported a vapor venting two-phase microchannel heat sink, in which a hydrophobic porous membrane was placed above the microchannels to dissipate vapor. Their experiments demonstrated that this approach can reduce the normalized flow pressure drop by 60 %. Mohiuddin et al. [29] experimentally investigated membrane venting flow boiling in a single mini-channel, examining the influence of the channel's width-to-depth ratio. Their results indicated that membrane vent can reduce the pressure drop in shallow channels by approximately 40–60 %, but has minimal impact on deeper channels. Li et al. [30] studied flow boiling in parallel microchannels and found that the membrane vent can not only reduce the pressure drop but also improve the pressure stability. However, studies on membrane-venting boiling are still few. Data at heat flux above 85 W/cm^2 is scarce, and investigations have focused on flow boiling with heat and mass transfer in horizontal directions with membrane pore sizes no above 0.5 μm.

For the thermal management of high heat flux devices, as presented in Fig. 1, we proposed a type of membrane-venting thin film boiling (MV-TFB) heat sink, inspired by pressure-driven transmembrane vaporization [31,32], membrane distillation [33,34], and microchannels [35,36], The heat sink primarily consists of a liquid plate, a layer of hydrophobic porous membrane, and a vapor plate. During its operation, a pump drives the liquid fluid into the thin film region on the upper surface of the liquid plate, wherein the liquid absorbs heat and vaporizes to vapor. A part of generated vapor permeates through the hydrophobic porous membrane vertically, flows through the vapor channels, and exits the heat sink via the vapor outlet. Additionally, the rest vapor horizontally flows out via the liquid outlet combining with the liquid phase. The hydrophobic porous membrane not only dissipates vapor but also keeps the thickness of the liquid region at the micron level.

Compared with existing microchannel flow boiling heat sinks employing membrane vent, the MV-TFB heat sink focuses on enhancing heat and mass transfer in the vertical direction more. Specific measures include: (a) for the hydrophobic porous membrane layer, selecting a larger pore size of 1.0 μm to reduce its intrinsic vapor resistance; (b) for the liquid plate, utilizing a slit as the flow structure instead of channels with fins to minimize effective membrane area loss due to the shade effect of fins; (c) for the vapor plate, the fins are needle-shaped and the distances between the fins are in the order of millimeters to reduce vapor resistance arising from the shade effect and viscous force. Experiments show that the heat and mass transfer mechanisms of the MV-TFB heat sink deviate from the horizontal flow boiling pattern. Remarkably, even under a high heat flux of 312.5 W/cm^2, the fluid at the liquid plate outlet can still be subcooled almost with no vapor, i.e., the vaporization mode was thin film boiling and thin film evaporation in the vertical direction.

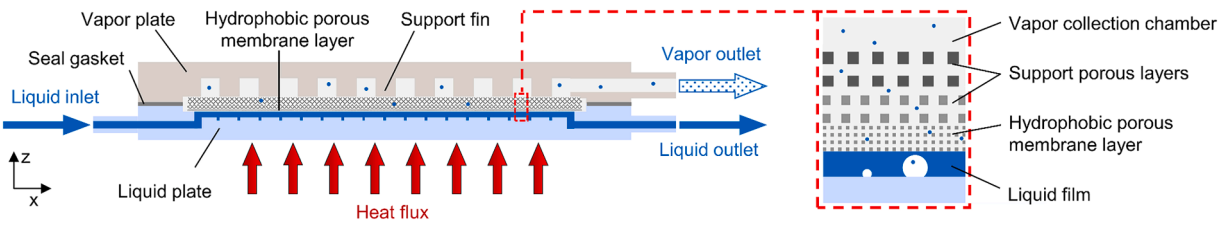

Fig. 1. Schematic diagram of membrane-venting thin film boiling (MV-TFB) heat sink.

The details of the experimental setup and results are described subsequently.

2. Experimental setup

2.1. Test loop

The working fluid used in the experiment was deionized water. Fig. 2 presents the schematic diagram of the test loop, primarily consists of a liquid reservoir, a vane pump (DC50H, Zhongke Century, Maximum head: 20 m), a filter (10 μm, Sanglian), a flowmeter (AK77, Yihai), an inlet temperature controller, a test section, an outlet cooler, an outlet condenser, a condensate collector, and a jet pump (SHB-IIIG). The liquid reservoir's mass change was measured by using a weighing scale (YP50001B, LICHEN). The inlet temperature controller is a plate heat exchanger, and the temperature of its working medium was controlled by a constant temperature bath (WD-1003D, BiLon). In the test section, for the inlet and outlet fluids of the heat sink, pressures were obtained via pressure gauges (Y80, SUX) and temperatures were measured by utilizing K-type thermocouples inserted into pipes. Temperatures at the liquid plate were also measured by K-type thermocouples. These temperature data were collected with a data acquisition system (2700, Keithley). The power of the heater was regulated by two power regulators (TDGC2–1kVA, RMSPD) and measured through two power meters (PF9800, EVERFINE). The outlet cooler and condenser are also plate heat exchangers, employing water as a cooling medium. The fluid outputs from the liquid plate outlet was cooled by the cooler and subsequently returned to the liquid reservoir. The vapor from the vapor plate outlet was condensed in the condenser and then collected in a conical flask. A jet pump is connected to the conical flask to assist the condenser in maintaining the vacuum pressure of the vapor outlet.

2.2. Test section and the heat sink

Fig. 3 illustrates the structure of the test section, and Table 1 presents the primary structural dimensions of the sink components. As shown in Fig. 3(a), the working membrane, a type of composite membrane consisting of a hydrophobic porous membrane layer and a support porous membrane layer, was placed between the liquid plate and the vapor plate. All experiment configurations arranged a layer of Titanium fiber felt above the composite membrane to strengthen the support. Besides, in certain configurations, to adjust the thickness of the liquid film, one or two additional Nylon mesh membranes were arranged between the composite membrane and the Titanium fiber felt. As shown in Fig. 3(a, b, d), both the liquid plate and vapor plate have bolt holes on their edge region. The two plates were tightened by bolts and sealed by a seal gasket. As shown in Fig. 3(b), the top surface of the liquid plate has an area for placing membranes, several channels for liquid distribution, and a thin film region with a size of 20.00 mm × 20.00 mm for heat dissipation. As presented in Fig. 3(c, e), there is a square base pillar at the bottom of the liquid plate for measuring the temperature gradient, and 3 × 2 temperature measurement holes are arranged symmetrically on both sides of this pillar. As shown in Fig. 3(e, f), to provide high heat flux, 6 × 2 cartridge heater holes are arranged on two sides of the heater block, which features a heat-gathering structure. To decrease the thermal contact resistance between the heat sink and the heater block,

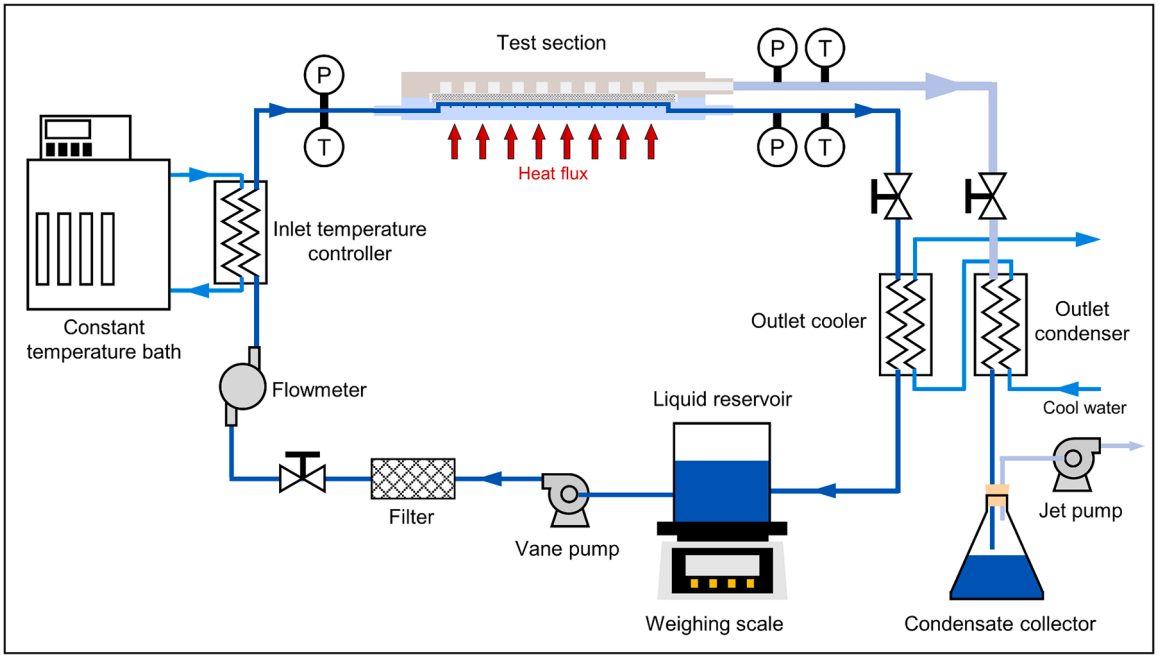

Fig. 2. Schematic diagram of test loop.

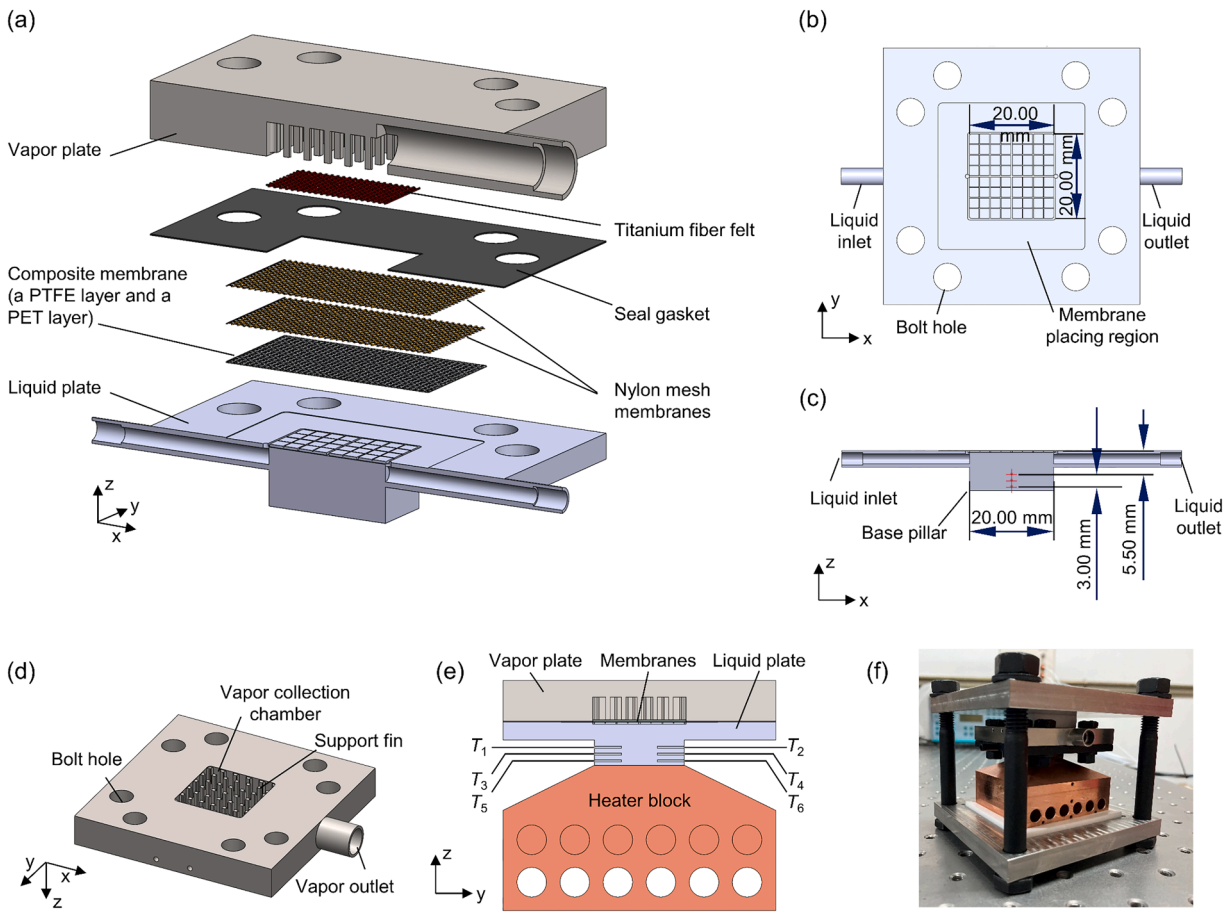

Fig. 3. Configuration of test section: (a) explosive view of heat sink; (b) top view of liquid plate; (c) side-sectional view of liquid plate; (d) vapor plate; (e) location of thermocouples on heat sink (side-sectional view); (f) photograph of test section (before assembling to test system).

Table 1
Main structural dimensions of sink components.

Component		Dimension	Value, mm
Liquid plate (Al 6063)	Thin film area	l (length) × w (width)	20.00 × 20.00
	Inlet/outlet channels	D (diameter)	3.00, 2.40, and 1.00
	Liquid distribution channels	w × dep (depth)	0.40 × 0.40, 0.25 × 0.40, and 0.17 × 0.17
	Base pillar	l × w × h (height)	20.00 × 20.00 × 5.60
	Thermometer holes	D × dep	0.50 × 6.00
Composite membrane	Hydrophobic layer (PTFE) + Support layer (PET)	l × w × thk (thickness)	31 × 31 × 0.16
Silicone membrane		l × w × thk	31 × 31 × 0.15
Nylon mesh membrane		l × w × thk	31 × 31 × 0.07
Titanium fiber felt		l × w × thk	20 × 20 × 0.13
Seal gasket (Silicone)		l × w × thk	60 × 60 × 0.07
Vapor plate (304 stainless steel)	Vapor collection chamber	l × w × dep	20.80 × 20.80 × 5.00
	Support fins	l × w × h	1.00 × 1.00 × 5.00
	Outlet channel	D	6.00 and 7.40

thermally conductive silicone grease (TF8, Thermalright, 13.8 W/m•K) was applied. Furthermore, as illustrated in Fig. 3(f), the heater block and heat sink were clamped by two clamping plates and four stud bolts. To reduce the impact of environmental heat dissipation, the heat sink and heater block were placed within an insulated enclosure after assembly, and the air gap inside the enclosure was filled by glass fiber wool.

2.3. Materials

The liquid plate, vapor plate, and heater block were manufactured from aluminum alloy 6063, stainless steel 304, and pure copper, respectively, using precision machining processes. As shown in Fig. 4(a), we had commissioned the processing manufacturer using sandblasting and anodizing to increase the surface roughness of the working area. All the used porous materials can be obtained inexpensively from a filter material market. For the working membrane layer direct contact with the liquid film, it should be porous and hydrophobic to allow vapor quickly permeating while forbidding liquid from passing through it. The material of the working layer was chosen as polytetrafluoroethylene (PTFE), which is intrinsically hydrophobic. Instead of single layer PTFE porous membranes that are soft and difficult to assemble, as shown in Fig. 4(b–f), composite membranes (PTFE, 0.22/0.45/1.0 μm, LONGJIN) with a bilayer structure were selected as the working membranes. These composite membranes consist of a PTFE hydrophobic porous layer as shown in Fig. 4(b–d) and a polyethyleneterephthalate (PET) porous support layer as shown in Fig. 4(f). For the three types of composite membranes used in the experiment, the pore sizes of the working layer are 0.22, 0.45, and 1.0 μm, respectively, and their water contact angles were measured to be 141±2°, 142±3°, and 142±3°, respectively (sessile drop method, DSA30, Kruss). The thickness and characteristics of the support layer of these composite membranes are the same. The pore sizes of PET layer, Nylon mesh membrane, and Titanium fiber felt are approximately tens of micrometers. So, the vapor transfer resistance of these support layers can be ignored compared with that of the working layer [27]. In single-phase flow convection or control experiment, the composite membrane was replaced with a silicone membrane that

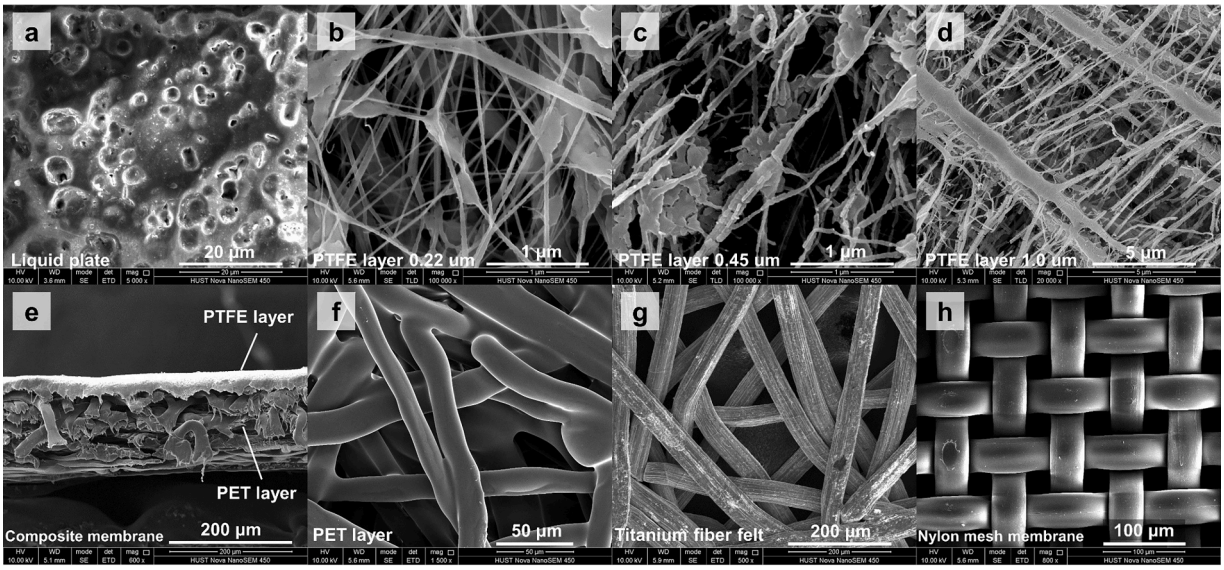

Fig. 4. SEM images of materials: **(a)** liquid plate surface; **(b-d)** hydrophobic porous membrane layer (PTFE, 0.22/0.45/1.0 μm); **(e)** cross-section view of composite membrane (a 0.22 μm PTFE layer with a PET support layer); **(f-h)** support porous layer (PET membrane layer, Titanium fiber felt, and Nylon mesh membrane).

forbids the permeation of both liquid and vapor.

2.4. Test process

Before the main experiments, we verified the accuracy of the effective heat power measurement by a single-phase convection experiment. Then, we investigated the effect of the pore size of the venting membrane by using a silicone membrane with a 0 μm pore size, or a composite membrane with PTFE layer pore sizes of 0.22/0.45/1.0 μm as working membrane, respectively. If employed a 2.0 μm PTFE membrane layer, due to the weaker surface tension, the larger pores can't resistant the liquid's permeation, and the liquid would quickly pass through the membrane and leave the loop, making the experiment unable to perform. In addition, we examined the influence of the liquid film thickness by adding additional Nylon mesh support membranes. Irrespective of material deformation, the liquid film thickness was approximately 0.18 mm for the configuration without the mesh membrane. After employing one or two mesh membranes as support porous layers, the liquid film thickness decreased to approximately 0.11 mm and 0.04 mm, respectively. Furthermore, we investigated the impact of the inlet flow rate by adjusting the inlet flow rate to 50, 100, or 150 mL/min, respectively.

During the experiment, the liquid reservoir was connected to the atmosphere, and the pressure at the sink liquid outlet was close to atmospheric pressure. The condenser and jet pump can control the pressure of the vapor outlet at a minimum of 2.9 kPa, which can be equivalent to a cold source of 23.3 °C. The inlet liquid temperature was controlled at 19±1 °C. For each configuration, the experiment began with a low input heat power of 50 W and progressed to higher heating powers. For a certain condition, when the fluctuation of T_1~T_6 was less than 0.5 °C within 3 min, the formal statistical stage was entered, and the experiment was continued for more than 5 min. After completing a condition test, the heating power was increased by approximately 50 W. To protect the membrane from high temperature, If T_1~T_6 or inlet pressure persistently rose and couldn't stabilize after increasing the heating power, we determined the working failure condition was reached and stopped the experiment. Besides, for safety reasons, if the heating power was too high, we would also stop increasing the power even if no sign of failure. So, the critical heat flux hasn't been measured during the experiment. The heating power range for most configurations was 50–1100 W, while some configurations had maximum heating powers of 1200–1300 W.

3. Data reduction

The heat power inputted to the heater block, Q_{in}, was measured by a power meter. Based on energy balance, Q_{in} can be divided by:

$$Q_{in} = Q_{eff} + Q_{loss} \tag{1}$$

where Q_{eff} is the effective heat to the heat sink, and Q_{loss} is the heat loss to the environment. Q_{eff} was determined from the temperature gradient of the sink base pillar:

$$Q_{eff} = Aq_{eff} \tag{2}$$

$$q_{eff} = k_{Al}\frac{(T_5 + T_6) - (T_1 + T_2)}{2\Delta z} \tag{3}$$

where q_{eff} is the effective heat flux to the sink, A is the cross-section area of the sink base pillar, k_{Al} is the thermal conductivity of aluminum alloy 6063, T_1, T_2, T_5, and T_6 are the measured temperatures of the test points shown in Fig. 3(e), respectively, and Δz (3.00 mm) is the z-direction distance between the test points T_1 and T_5 as well as T_2 and T_6.

For the test configuration of single-phase convection, the effective heat input can also be calculated from the temperature difference between the inlet and outlet:

$$Q'_{eff} = \rho \dot{V} C_p (T_{out} - T_{in}) \tag{4}$$

where Q'_{eff} is the effective heat absorbed by the fluid, $\dot{V}$, T_{in}, T_{out} are the inlet rate, inlet temperature, outlet temperature, respectively, C_p and ρ are the specific heat and density of liquid water, respectively,

According to one-dimensional heat conduction assumption, the wall temperature at the thin film region, T_{wall} was estimated as:

$$T_{wall} = \frac{T_1 + T_2}{2} - \frac{q_{eff}\Delta z'}{k_{Al}} \tag{5}$$

where $\Delta z'$ (5.50 mm) is z-direction distance between the wall and the test point T_1 as well as T_2.

The pressure drop of the sink, ΔP was calculated as:

$$\Delta P = P_{in} - P_{out} \tag{6}$$

where P_{in} and P_{out} are measured pressures at the inlet and the outlet, respectively.

The transmembrane mass flux, J_{mem} was calculated as:

$$J_{mem} = -\frac{\Delta m}{A\Delta t} \tag{7}$$

where Δm is the fluid mass change of the cycle, measured from the liquid reservoir weight, and Δt is the measured interval.

The transmembrane heat flux, q_{mem} was estimated as:

$$q_{mem} = J_{mem}\left(C_p(T_{out} - T_{in}) + H_{lv}\right) \tag{8}$$

where H_{lv} is the latent heat of vaporization.

The average vapor quality of the two sink outlets, χ was estimated as:

$$\chi = \frac{Q_{eff} - \rho\dot{V}C_p(T_{out} - T_{in})}{\rho\dot{V}H_{lv}} \tag{9}$$

The uncertainties of the measured parameters are listed in Table 2. The uncertainties of the calculated parameters were estimated based on the common method and are listed in Table 2 [37].

4. Results and discussion

4.1. Accuracy verification of measured heat flux

Fig. 5 presents the effective heat obtained in the single-phase convection experiment. For this configuration, the inlet rate was maintained at 150 mL/min and the working membrane was a silicone membrane with pore size of 0 μm to minimize the venting effect. Experiment results indicate that the Q_{eff} deduced from the temperature gradient of the sink base pillar and the Q'_{eff} calculated from the temperature difference between the inlet and outlet are close to each other, testified the reliability of measured heat flux. Besides, the heat sink operated stably when Q_{in} was not higher than 800 W. However, when Q_{in} increased to 850 W, many vapor bubbles started to appear in the liquid outlet accompanied by a continuous rise in P_{in}. After P_{in} rising to the limit of the vane pump, the system still couldn't be stabilized. Consequently, the inlet rate declined and the heat sink failed.

4.2. Influence of the venting membrane pore size

Experiment results show that MV-TFB can effectively address high flux heat dissipation, and a larger pore size of the venting membrane significantly benefits the MV-TFB heat sink to dissipate a higher heat flux and reduce the pressure drop. Fig. 6 presents the wall temperature, T_{wall}, liquid outlet temperature, T_{out}, pressure drop, ΔP, and transmembrane mass flux, J_{mem}, for working membrane pore size of 0, 0.22, 0.45, and 1.0 μm, respectively, in relation to the effective heat flux, q_{eff}. Fig. 7 shows the transmembrane heat flux, q_{mem}, and average vapor quality, χ, of the two sink outlets when q_{eff} was at its maximum. The inlet rates were kept at 50 mL/min during these test conditions. The results indicate that T_{wall}, T_{out}, and J_{mem} were not sensitive to the membrane pore size under a similar q_{eff}. However, with the membrane of a larger pore size, the heat sink can work stably at a higher heat flux while

Table 2
Uncertainties of parameters.

Measured parameter	Uncertainty	Calculated parameter	Uncertainty
Q_{in}	±0.5 %	Q_{eff}	±14 W
T_{in}, T_{out}	±0.5 °C	Q'_{eff}	±16 W
T_1~T_6	±0.5 °C	q_{eff}	±3.4 W/cm^2
P_{in}, P_{out}	±0.2 kPa	T_{wall}	±1.2°C
$\dot{V}$	±3 mL/min	ΔP	±0.3 kPa
m	±0.1 g	J_{mem}	±0.01$kg/m^2{\cdot}s$

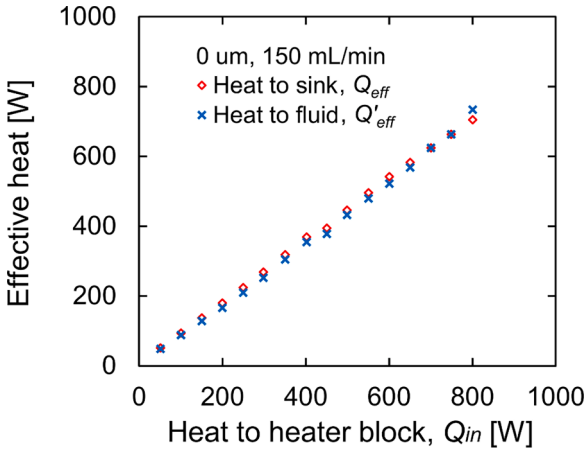

Fig. 5. Effective heat versus input heat to heater block at single-phase experiment with working membrane pore size of 0 μm and inlet rate of 150 mL/min.

achieving higher transmembrane fluxes and a vaporization ratio. Furthermore, the pressure drop was also reduced at a high heat flux. For the configuration of silicone membrane (0 μm) with no venting effect, the maximum effective heat flux, $q_{eff,max}$ was only 44.1 W/cm^2. If under a higher heat flux such as about 55 W/cm^2, the pressure drop increased very rapidly, and even the pump owning a pumping ability of 200 kPa couldn't supply liquid to the thin film region, leading to work failure. For the configuration with venting membrane of a 1.0 μm pore size, the effective heat flux achieved 287.8 W/cm^2 with the transmembrane heat flux of 152.7 W/cm^2, where the heat transfer in the vertical direction contributed over half of the total dissipated heat. χ also reached a high value of 0.46. Compared to the 0 μm configuration, $q_{eff,max}$ increased by 553 %, and compared to the 0.22 μm configuration, $q_{eff,max}$ increased by 65 %. Besides, when q_{eff} was about 175 W/cm^2, the 1.0 μm configuration can reduce the pressure drop loss by 62 % compared with the 0.2 μm configuration.

4.3. Working regimes of MV-TFB heat sink

As shown in Fig. 8, the vaporization modes of the MV-TFB heat sink should comprise boiling near the wall surface and evaporation at the membrane-liquid interface. According to whether the wall surface temperature and the liquid outlet temperature are higher than the saturation temperature, the working regime can be divided into single-phase convection (SPC), two-phase convection with subcooled boiling (TPC-SCB), and two-phase convection with saturated boiling (TPC-STB). As presented in Fig. 6, when q_{eff} was about 0–45 W/cm^2, both T_{wall} and T_{out} were below the saturation temperature, and the regime was SPC. In this regime, as the heat flux increased, T_{wall} and T_{out} increased fast, J_{mem} increased slowly, while ΔP was lower and varied minimally. When q_{eff} was about 55–100 W/cm^2, T_{wall} exceeded the saturation temperature while T_{out} remained lower than the saturation temperature, and the regime was TPC-SCB. In this regime, subcooled boiling occurs at the wall surface. As a boiling phenomenon in a microscale confine region, the size of the bubbles should be comparable to the thin liquid film. So the vapor generated at the wall surface can not only heat the fluid, thus enhancing the evaporation at the membrane-liquid interface, but aslo directly crossed the membrane and exited the sink through the vapor outlet. Therefore, the heat dissipation ability became stronger, and as the heat flux increased, T_{wall} and T_{out} rose slowly while J_{mem} rose fast. Because the fluid was subcooled and had a low vapor quality, ΔP didn't rise significantly with the heat flux. In addition, due to the low vapor quality of the thin film, the venting capacity of the hydrophobic porous membrane was not yet a limiting factor for J_{mem}, making J_{mem} less sensitive to the pore size. When q_{eff} was above 100 W/cm^2, T_{out} reached the saturation temperature and the regime transitioned to TPC-STB. Under

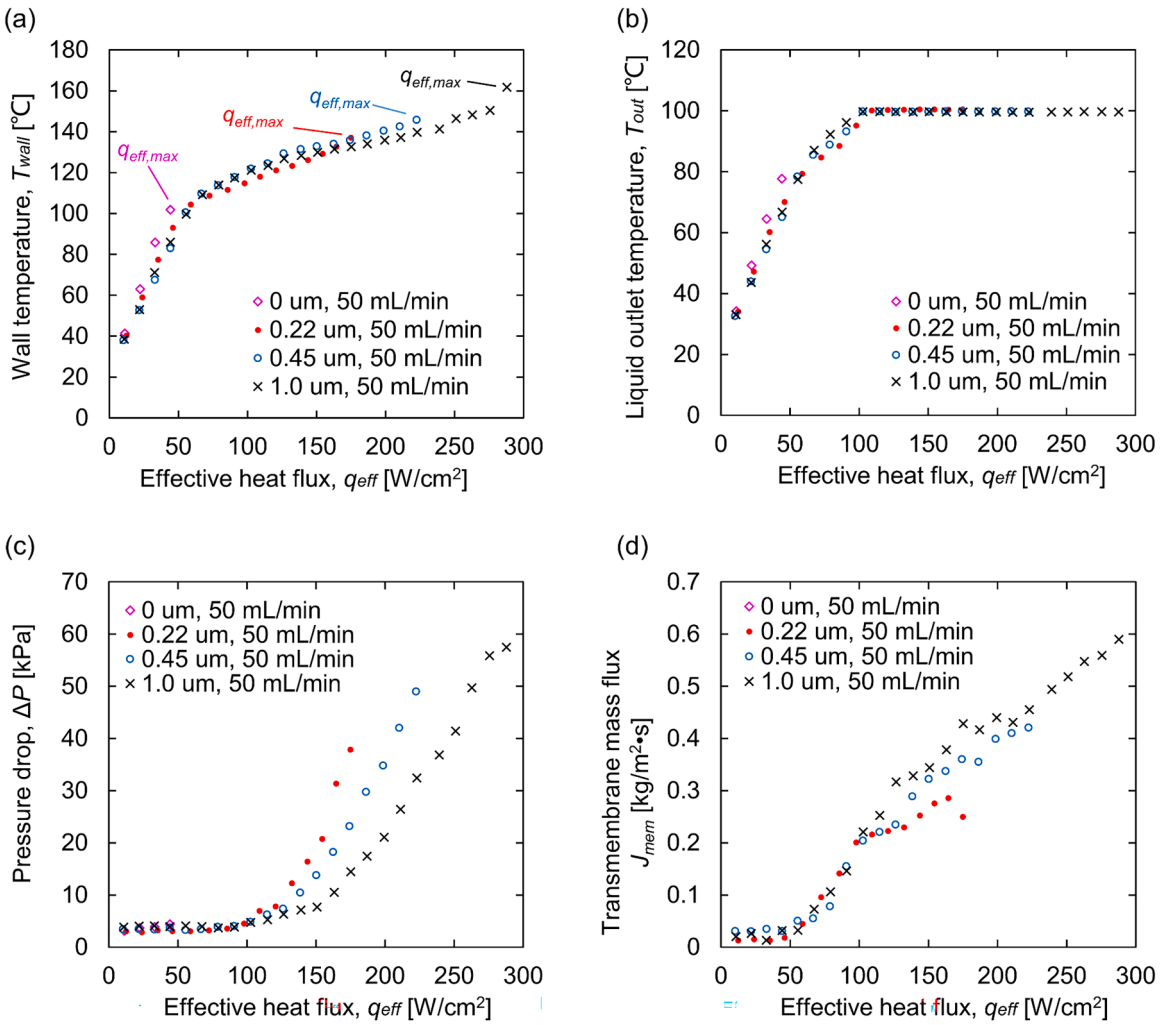

Fig. 6. Characteristics versus effective heat flux with venting membrane pore sizes of 0, 0.22, 0.45, 1.0 μm and under inlet rate of 50 mL/min: **(a)** wall temperature; **(b)** liquid outlet temperature; **(c)** pressure drop; **(d)** transmembrane mass flux.

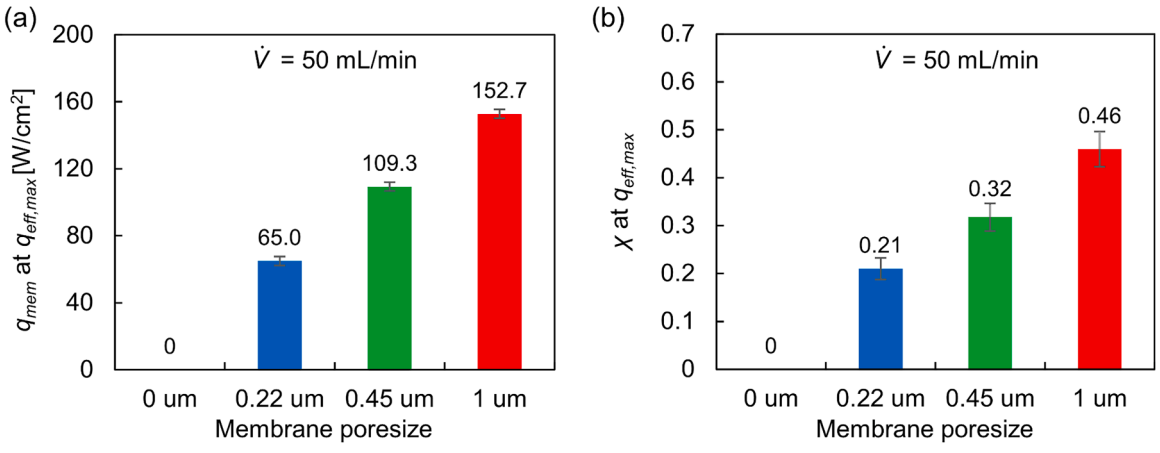

Fig. 7. Transmembrane heat flux, J_{mem} and outlet vapor quality, χ under maximum effective heat flux with pore sizes of 0, 0.22, 0.45, 1.0 μm and inlet rate of 50 mL/min: **(a)** J_{mem}; **(b)** χ.

this regime, boiling heat transfer became intense. As the heat flux rose, T_{wall} rose slowly and J_{mem} increased quickly. However, with the rise of vapor quality in the liquid plate, the accelerated and frictional pressure drop increased. Thus, ΔP rose rapidly with heat flux. The fluid in the liquid plate was saturated, and the vapor generated by boiling at the local region can transfer horizontally to a long distance, thereby exerting a greater influence on flow and vaporization. Therefore, the venting capacity of the membrane strongly impacted ΔP and $q_{eff,max}$.

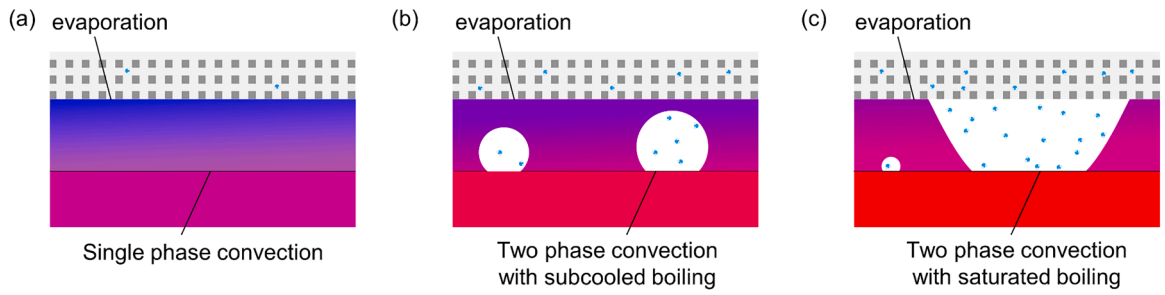

Fig. 8. Schematic diagrams of working regimes: **(a)** single-phase convection, SPC; **(b)** two-phase convection with subcooled boiling, TPC-SCB; **(c)** two-phase convection with saturated boiling, TPC-STB.

4.4. *Influence of the liquid film thickness*

A too thin thickness of the liquid film negatively affects the MV-TFB heat sink, which has little impact on heat transfer performance but significantly increases pressure drop. Fig. 9 presents the characteristics of the MV-TFB heat sink versus effective heat flux for configurations with 0, 1, and 2 layers of Nylon mesh support membranes, respectively. As mentioned before, the liquid film thickness for these configurations was approximately 0.18, 0.11, and 0.04 mm, respectively. These configurations employed working membranes with a 0.45 μm pore size in hydrophobic layers. The inlet rate was kept at 100 mL/min. The experimental results show that benefiting from the large inlet rate, these configurations didn't exhibit signs of failure with the effective heat flux at 260.6–282.2 W/cm^2. Due to the limitation of the heater, the maximum effective heat fluxes of those configurations had not been measured yet. When q_{eff} was 0–90 W/cm^2, 90–200 W/cm^2, and above 200 W/cm^2, the working regime was SPC, TPC-SCB, and TPC-STB, respectively. Reducing the liquid film thickness can slightly improve the heat transfer in the SPC regime, resulting in a slight decrease in T_{wall}, but it also slightly worsened the heat and mass transfer performance in the TPC stage, leading to a small increase in T_{wall}, a small decrease in J_{mem} and, most critically, a large increase in ΔP. Under the test condition

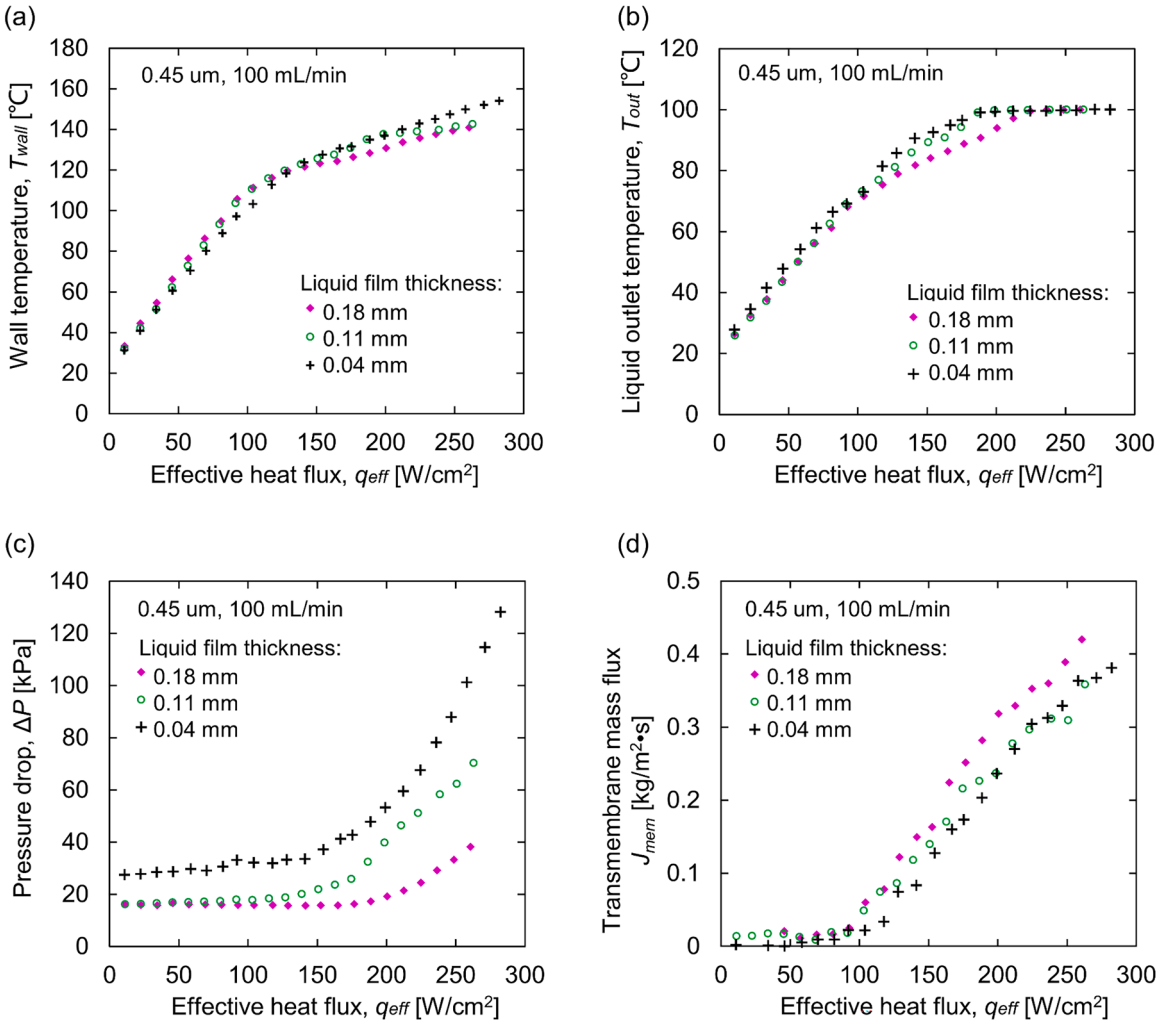

Fig. 9. Characteristics versus effective heat flux with liquid film thickness of 0.18, 0.11, or 0.04 mm, venting layer pore size of 0.45 μm, and inlet rate of 100 mL/min: **(a)** wall temperature; **(b)** liquid outlet temperature; **(c)** pressure drop; **(d)** transmembrane mass flux.

with the effective heat flux of 257.9–260.6 W/cm^2, the ΔP of the configuration with a 0.04 mm film thickness was 165 % higher than that of the configuration with a 0.18 mm film thickness.

4.5. Influence of fluid supply rate

Increasing the inlet rate substantially improves the heat transfer performance of the MV-TFB heat sink. Fig. 10 shows the heat sink characteristics with the effective heat flux for inlet rates of 50, 100, and 150 mL/min, respectively. These curves are from the same configuration with a venting membrane pore size of 1.0 μm. The experimental results show that increasing the inlet rate suppressed the transition of the regime from SPC to TPC-SCB and TPC-STB, resulting in slower increase rates in T_{wall}, T_{out}, ΔP, and J_{mem} as q_{eff} increases. At lower q_{eff}, the regime was dominated by SPC. An increase in the inlet rate significantly reduced the wall temperature, but it also significantly increased the pressure drop. When q_{eff} was 44.2–45.9 W/cm^2, compared to the condition with an inlet rate of 50 mL/min, increasing the inlet rate to 150 mL/min reduced T_{wall} from 85.9 °C to 56.9 °C, however, ΔP also increased from 4.0 kPa to 32.7 kPa. When q_{eff} was high, increasing the inlet rate suppressed TPC, resulting in slower increase rates of T_{wall}, T_{out}, ΔP, and J_{mem} with increasing q_{eff}, which was conducive to avoiding failure. For the condition with an inlet rate of 50 mL/min, when q_{eff} was 287.8 W/cm^2, T_{wall} was 161.8 °C, ΔP was 57.5 kPa, and further increasing heat flux resulted in failure. For the 150 mL/min condition, when q_{eff} was 288.5 W/cm^2, T_{wall} was 136.2 °C, and ΔP was 37.0 kPa, which reduced T_{wall} by 25.6 °C, and ΔP by 20.5 kPa, respectively. Moreover, when q_{eff} further increased to 312.5 W/cm^2, the fluid at the liquid outlet was still in a subcooled state, and the regime was still TPC-SCB, not yet transformed to TPC-STB. At a such high heat flux, the vaporization model was still thin film subcooled boiling and evaporation. This result implies that the MV-TFB heat sink has the potential to deal with the heat flux of several hundreds of watts per square centimeter.

5. Discussion

Compared to existing research on membrane-venting microchannels, this work has achieved heat fluxes of over 100 W/cm^2, demonstrating that membrane-venting boiling is an effective approach for high heat flux device thermal management [29,30,31], Furthermore, this work demonstrates that increasing the pore size of the venting membrane can significantly improve pressure drop and critical heat flux. Mohiuddin et al. [30] conducted experiments using membranes with pore sizes of 0.22 and 0.45 μm but did not observe a significant influence of pore size on pressure drop and heat transfer. They explained that the permeability of these two membranes was roughly comparable. For the membranes with pore sizes of 0.22, 0.45, and 1.0 μm used in this study, according to the supplier's data, the transmembrane fluxes of liquid alcohol are 0.51, 0.63, and 1.38 mL/cm^2/min/kPa, respectively, indicating distinct transfer capabilities. Therefore, as shown in Figs. 6 and 7, the adoption of membranes with larger pore sizes led to significant improvements in critical heat flux, pressure drop, and transmembrane flux.

Based on the results of this study and other existing research [28,29,30], membrane-vent can greatly enhance the performance of flow boiling, particularly in terms of reducing pressure drop and increasing critical heat flux. Therefore, further investigation of membrane-venting boiling is highly meaningful. Engineering implementation of

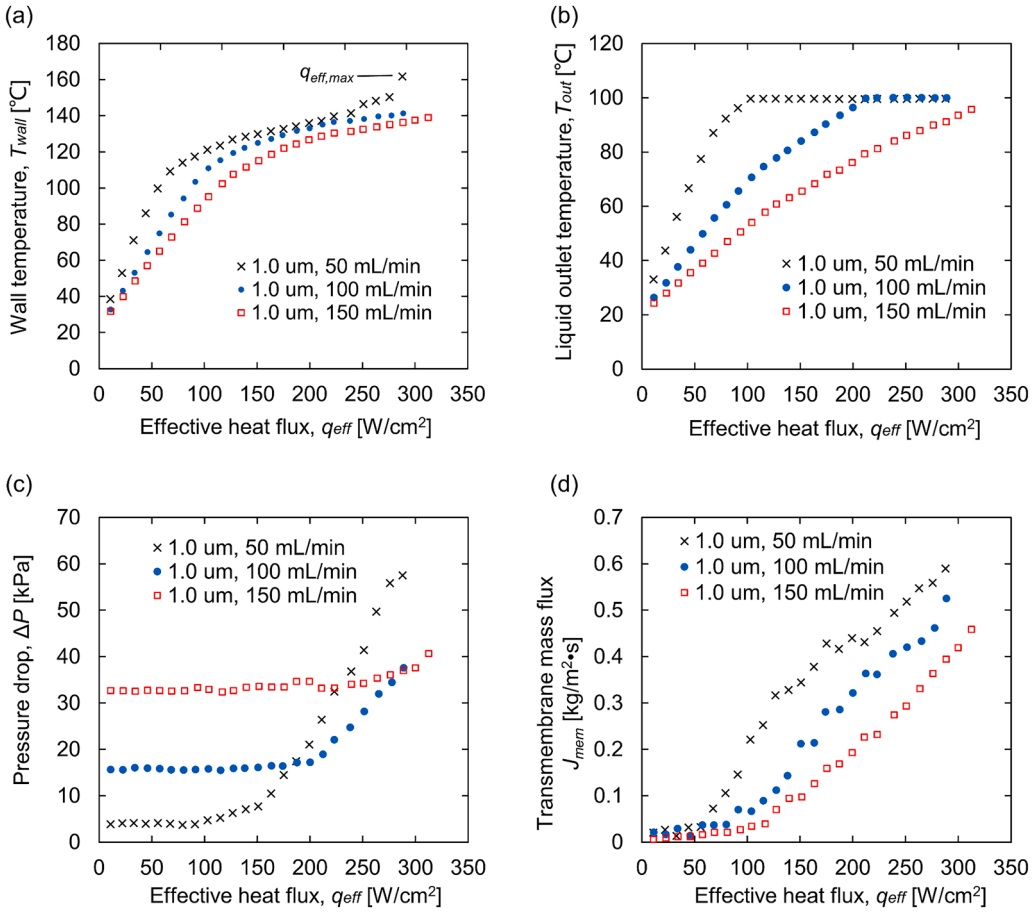

Fig. 10. Characteristics versus effective heat flux with venting membrane pore size of 1.0 μm, and under inlet rate of 50, 100, 150 mL/min: **(a)** wall temperature; **(b)** liquid outlet temperature; **(c)** pressure drop; **(d)** transmembrane mass flux.

membrane-venting heat sink is not complex, as it involves some modifications to the structure and piping of conventional microchannel thermal management systems [28]. Although the thickness dimension slightly increases, the heat sink still maintains good compactness without affecting its application in most scenarios. As membrane-vent is the approach that adds heat and mass transfer pathways in the vertical direction, membrane-vent is compatible with many flow boiling enhancement techniques. It is necessary to further explore the influence of flow structure optimization [29,30], surface treatment, and membrane optimization on the two-phase characteristics of membrane-venting heat sinks. In this study, to facilitate the measurement of the working fluid's mass change, the test loop was not designed as a closed system. Under this condition, the boiling point of water is approximately 100 °C, while the heat dissipation capacity still meets the requirements of devices with good temperature resistance such as IGBTs. If necessary to control a device at a lower temperature, the boiling point needs to be reduced by lowering the system pressure to promote early occurrence of boiling heat transfer. Therefore, further study of membrane-venting heat sinks with low working pressure is very necessary.

6. Conclusions

This study experimentally investigated the heat and mass transfer characteristics of a membrane-venting thin film boiling (MV-TFB). The effective area of the heat sink is 20.00 mm × 20.00 mm. The effect of venting membrane pore size was examined by using a silicone membrane with 0 μm pore size and PTFE hydrophobic membranes with 0.22/0.45/1.0 μm pore sizes. The effect of liquid film thickness was also investigated by adjusting it to about 0.04/0.11/0.18 mm. In addition, the effect of the inlet rate was investigated by adjusting it to 50, 100, or 150 mL/min. The main conclusions of this study are as follows:

1. Membrane venting is an effective way to improve flow boiling. Compared to thin film flow boiling (TFFB), MV-TFB has an additional vertical heat and mass transfer channel, which alleviates the failure of horizontal flow boiling and increases the heat dissipation capacity. At an inlet rate of 50 mL/min, MV-TFB with a 1.0 μm pore-size membrane can dissipate an effective heat flux of up to 287.8 W/cm^2, which is 5.5 times higher than that of TFFB;
2. MV-TFB heat sink has relatively poor heat dissipation performance under the single-phase convection regime, with small transmembrane heat and mass fluxes. When subcooled boiling or saturated boiling occurs in the liquid film, the heat and mass transfer ability of the MV-TFB heat sink becomes stronger. As the heat flux increases, the wall temperature rises slowly and the transmembrane fluxes rise quickly;
3. Increasing the pore size of the hydrophobic membrane and the inlet rate can significantly improve the heat transfer performance of the MV-TFB heat sink. In addition, reducing the liquid film thickness has little effect on its heat transfer performance, but significantly increases the pressure drop. For the condition with a hydrophobic membrane pore size of 1.0 μm, a liquid film thickness of approximately 0.18 mm, and an inlet rate of 150 mL/min, the MV-TFB heat sink can dissipate a high effective heat flux of 312.5 W/cm^2 while the liquid at the outlet was still in a subcooled state.

Funding sources

The study is supported by the National Natural Science Foundation of China (No. 52076088).

Declaration of Competing Interest

The authors declare that they have no known competing financial interests or personal relationships that could have appeared to influence the work reported in this paper.

Data availability

Data will be made available on request.

References

[1] J.L. Smoyer, P.M. Norris, Brief historical perspective in thermal management and the shift toward management at the nanoscale, Heat Transf. Eng. 40 (2019) 269–282, https://doi.org/10.1080/01457632.2018.1426265.
[2] T.G. Karayiannis, M.M. Mahmoud, Flow boiling in microchannels: fundamentals and applications, Appl. Therm. Eng. 115 (2017) 1372–1397, https://doi.org/10.1016/j.applthermaleng.2016.08.063.
[3] P. Wang, P. Mccluskey, A. Bar-Cohen, Two-phase liquid cooling for thermal management of igbt power electronic module, J. Electron. Packag. Trans. ASME. 135 (2013), 021001, https://doi.org/10.1115/1.4023215.
[4] P. Cui, Z. Liu, Experimental study on flow boiling in ultrahigh-aspect-ratio copper microchannel heat sink, Appl. Therm. Eng. 223 (2023), 119975, https://doi.org/10.1016/j.applthermaleng.2023.119975.
[5] M. Morisaki, S. Minami, K. Miyazaki, T. Yabuki, Direct local heat flux measurement during water flow boiling in a rectangular minichannel using a MEMS heat flux sensor, Exp. Therm. Fluid Sci. 121 (2021), 110285, https://doi.org/10.1016/j.expthermflusci.2020.110285.
[6] M. Chernysheva, S. Vershinin, Y. Maydanik, Development and investigation of a loop heat pipe at a high concentration of heat load, Int. J. Heat Mass Transf. 197 (2022), 123316, https://doi.org/10.2139/ssrn.4045891.
[7] K. Nakamura, A. Ueno, H. Nagano, Experimental study on long-distance anti-gravity loop heat pipe with submicron-scale porous structure, Appl. Therm. Eng. 214 (2022), 122950, https://doi.org/10.1016/j.applthermaleng.2022.118793.
[8] S. Mori, N. Maruoka, K. Okuyama, Critical heat flux enhancement by a two-layer structured honeycomb porous plate in a saturated pool boiling of water, Int. J. Heat Mass Transf. 118 (2018) 429–438, https://doi.org/10.1016/j.ijheatmasstransfer.2017.10.100.
[9] N. Unno, R. Noma, K. Yuki, S. ichi Satake, K. Suzuki, Effects of surface properties on wall superheat at the onset of microbubble emission boiling, Int. J. Multiph. Flow. 155 (2022), 104196, https://doi.org/10.1016/j.ijmultiphaseflow.2022.104196.
[10] X. Li, S. Wang, R. Wen, X. Ma, R. Yang, Liquid film boiling enabled ultra-high conductance and high flux heat spreaders, Cell Reports Phys. Sci. 3 (2022), 100746, https://doi.org/10.1016/j.xcrp.2022.100746.
[11] L. Chen, F. Jin, J. Li, Y. Lv, Q. Wang, D. Zheng, H. Xian, J. Lin, Hybrid model of thin film boiling: insights into the unique behavior and ultrahigh heat flux, Int. J. Heat Mass Transf. 179 (2021), 121702, https://doi.org/10.1016/j.ijheatmasstransfer.2021.121702.
[12] T. Hikata, H. Fujimoto, Evaluating surface heat flux in planar water-jet cooling of moving hot solid by inversely solving steady-state heat conduction, Int. J. Heat Mass Transf. 197 (2022), 123364, https://doi.org/10.1016/j.ijheatmasstransfer.2022.123364.
[13] H.C. Cui, X.T. Lai, J.F. Wu, M.Z. Wang, W. Liu, Z.C. Liu, Overall numerical simulation and experimental study of a hybrid oblique-rib and submerged jet impingement/microchannel heat sink, Int. J. Heat Mass Transf. 167 (2021), 120839, https://doi.org/10.1016/j.ijheatmasstransfer.2020.120839.
[14] C. Park, J. Seol, A. Aldalbahi, M. Rahaman, A.L. Yarin, S.S. Yoon, Drop impact phenomena and spray cooling on hot nanotextured surfaces of various architectures and dynamic wettability, Phys. Fluids. 35 (2023), 027126, https://doi.org/10.1063/5.0139960.
[15] R.J. Ji, D.Q. Zhu, X.W. Lin, Z.F. Zhou, B. Chen, Parametric investigation on the close-loop R410A flash spray system for high power electronics cooling under low temperature, Case Stud. Therm. Eng. 41 (2023), 102643, https://doi.org/10.1016/j.csite.2022.102643.
[16] H. Sadique, Q. Murtaza, Samsher, Heat transfer augmentation in microchannel heat sink using secondary flows: a review, Int. J. Heat Mass Transf. 194 (2022), 123063, https://doi.org/10.1016/j.ijheatmasstransfer.2022.123063.
[17] Y.K. Prajapati, P. Bhandari, Flow boiling instabilities in microchannels and their promising solutions – A review, Exp. Therm. Fluid Sci. 88 (2017) 576–593, https://doi.org/10.1016/j.expthermflusci.2017.07.014.
[18] W. Qu, I. Mudawar, Measurement and correlation of critical heat flux in two-phase micro-channel heat sinks, Int. J. Heat Mass Transf. 47 (2004) 2045–2059, https://doi.org/10.1016/j.ijheatmasstransfer.2003.12.006.
[19] B. Wang, Y. Hu, Y. He, N. Rodionov, J. Zhu, Dynamic instabilities of flow boiling in micro-channels: a review, Appl. Therm. Eng. 214 (2022), 118773, https://doi.org/10.1016/j.applthermaleng.2022.118773.
[20] D. Deng, L. Chen, W. Wan, T. Fu, X. Huang, Flow boiling performance in pin fin-interconnected reentrant microchannels heat sink in different operational conditions, Appl. Therm. Eng. 150 (2019) 1260–1272, https://doi.org/10.1016/j.applthermaleng.2019.01.092.
[21] S.G. Kandlikar, T. Widger, A. Kalani, V. Mejia, Enhanced flow boiling over open microchannels with uniform and tapered gap manifolds, J. Heat Transfer. 135 (2013), 061401, https://doi.org/10.1115/1.4023574.
[22] A. Priy, S. Raj, M. Pathak, M.K. Khan, A hydrophobic porous substrate-based vapor venting technique for mitigating flow boiling instabilities in microchannel heat

sink, Appl. Therm. Eng. 216 (2022), 119138, https://doi.org/10.2139/ssrn.4024169.
[23] T. Alam, W. Li, W. Chang, F. Yang, J. Khan, C. Li, A comparative study of flow boiling HFE-7100 in silicon nanowire and plainwall microchannels, Int. J. Heat Mass Transf. 124 (2018) 829–840, https://doi.org/10.1016/j.ijheatmasstransfer.2018.04.010.
[24] X. Jiang, S.Waqar Ali Shah, J. Liu, Y. Li, S. Zhang, Z. Wang, C. Pan, Design of micro-nano structures for counter flow diverging microchannel heat sink with extraordinarily high energy efficiency, Appl. Therm. Eng. 209 (2022), 118229, https://doi.org/10.1016/j.applthermaleng.2022.118229.
[25] L. Yin, M. Sun, P. Jiang, C. Dang, L. Jia, Heat transfer coefficient and pressure drop of water flow boiling in porous open microchannels heat sink, Appl. Therm. Eng. 218 (2023), 119361, https://doi.org/10.1016/j.applthermaleng.2022.119361.
[26] K. Fu, W. Gao, X. Xu, X. Liang, Flow boiling heat transfer and pressure drop characteristics of water in a copper foam fin microchannel heat sink, Appl. Therm. Eng. 218 (2023), 119295, https://doi.org/10.1016/j.applthermaleng.2022.119295.
[27] K.W. Lawson, D.R. Lloyd, Membrane distillation, J. Memb. Sci. 124 (1997) 1–25, https://doi.org/10.1016/S0376-7388(96)00236-0.
[28] M.P. David, J. Miler, J.E. Steinbrenner, Y. Yang, M. Touzelbaev, K.E. Goodson, Hydraulic and thermal characteristics of a vapor venting two-phase microchannel heat exchanger, Int. J. Heat Mass Transf. 54 (2011) 5504–5516, https://doi.org/10.1016/j.ijheatmasstransfer.2011.07.040.
[29] A. Mohiuddin, R. Loganathan, S. Gedupudi, Experimental investigation of flow boiling in rectangular mini/micro-channels of different aspect ratios without and with vapour venting membrane, Appl. Therm. Eng. 168 (2020), 114837, https://doi.org/10.1016/j.applthermaleng.2019.114837.
[30] S. Li, M. Wei, Experimental study on flow boiling characteristics in continuous and segmented microchannels with vapor venting membrane, Energies 15 (2022) 8756, https://doi.org/10.3390/en15228756.
[31] J. Li, R. Long, B. Zhang, R. Yang, W. Liu, Z. Liu, Nano heat pump based on reverse thermo-osmosis effect, J. Phys. Chem. Lett. 11 (2020) 9856–9861, https://doi.org/10.1021/acs.jpclett.0c02475.
[32] Q. Wang, R. Chen, Ultrahigh flux thin film boiling heat transfer through nanoporous membranes, Nano Lett. 18 (2018) 3096–3103, https://doi.org/10.1021/acs.nanolett.8b00648.
[33] Y. Zhang, J. Li, Z. Zhang, W. Liu, Z. Liu, Enhancing thermo-osmotic low-grade heat recovery by applying a negative pressure to the feed, Glob. Challenges. 7 (2023), 2200238, https://doi.org/10.1002/gch2.202200238.
[34] J. Li, Z. Zhang, R. Zhao, B. Zhang, Y. Liang, R. Long, W. Liu, Z. Liu, Stack thermo-osmotic system for low-grade thermal energy conversion, ACS Appl. Mater. Interfaces. 13 (2021) 21371–21378, https://doi.org/10.1021/acsami.1c03395.
[35] X. Jiang, S. Zhang, Y. Li, Z. Wang, C. Pan, Achieving ultra-high coefficient of performance of two-phase microchannel heat sink with uniform void fraction, Int. J. Heat Mass Transf. 184 (2022), 122300, https://doi.org/10.1016/j.ijheatmasstransfer.2021.122300.
[36] Y. Zhang, Y. Fan, Z. Liu, W. Liu, Experimental and numerical study on two-phase minichannel cold plate for high-power device, Appl. Therm. Eng. 230 (2023), 120704, https://doi.org/10.1016/j.applthermaleng.2023.120704.
[37] J.R. Taylor, M.D. Semon, J.K. Pribram, Post-use review: an introduction to error analysis: the study of uncertainties in physical measurements, Am. J. Phys. 51 (1983) 191–192, https://doi.org/10.1119/1.13309.